

# Spring greening reduces autumnal runoff across high northern latitudes

Yongshuo Fu

yfu@bnu.edu.cn

Beijing Normal University <https://orcid.org/0000-0002-9761-5292>

Shouzhi Chen

Philippe Ciais

CEA CNRS UVSQ, Centre d'Etudes Orme des Merisiers <https://orcid.org/0000-0001-8560-4943>

Marcos Fernández-Martínez

CREAF

Zhenhong Hu

Northwest A&F University

Zitong Jia

Beijing Normal University

Xu Lian

Peking University <https://orcid.org/0000-0002-1428-3529>

Josep Peñuelas

CREAF-CSIC <https://orcid.org/0000-0002-7215-0150>

Chong-Yu Xu

University of Oslo <https://orcid.org/0000-0003-4826-5350>

Jing Tang

University of Copenhagen <https://orcid.org/0000-0001-7961-8214>

---

Biological Sciences - Article

Keywords:

Posted Date: April 6th, 2026

DOI: <https://doi.org/10.21203/rs.3.rs-9131543/v1>

License:   This work is licensed under a Creative Commons Attribution 4.0 International License.

[Read Full License](#)

**Additional Declarations:** There is **NO** Competing Interest.



# 1 **Spring greening reduces autumnal runoff across high northern latitudes**

## 2 **Authors**

3 Shouzhi Chen<sup>1</sup>, Yongshuo H. Fu<sup>1,2\*</sup>, Philippe Ciais<sup>3</sup>, Marcos Fernández-Martínez<sup>4</sup>,  
4 Zhenghong Hu<sup>4,5,6</sup>, Zitong Jia<sup>1</sup>, Xu Lian<sup>7</sup>, Josep Peñuelas<sup>4,8</sup>, Chongyu Xu<sup>9</sup>, Jing  
5 Tang<sup>10</sup>

## 6 **Affiliations**

7 <sup>1</sup>College of Water Sciences, Beijing Normal University, Beijing, China.

8 <sup>2</sup>Plants and Ecosystems, Department of Biology, University of Antwerp, Antwerp, Belgium.

9 <sup>3</sup>Laboratoire des Sciences du Climat et de l'Environnement, IPSL-LSCE,  
10 CEA/CNRS/UVSQ/Université Paris Saclay, Orme des Merisiers, Gif sur Yvette, France

11 <sup>4</sup>CREAF, Campus de Bellaterra (UAB), Cerdanyola del Vallès, Spain.

12 <sup>5</sup>State Key Laboratory of Soil Erosion and Dryland Farming on the Loess Plateau, College of Soil  
13 and Water Conservation Science and Engineering, Northwest A&F University, Yangling, Shaanxi,  
14 China.

15 <sup>6</sup>Shenzhen Research Institute, Northwest A&F University, Shenzhen, Guangdong, China.

16 <sup>7</sup>Institute of Carbon Neutrality, Sino-French Institute for Earth System Science, College of Urban  
17 and Environmental Sciences, Peking University, Beijing, China

18 <sup>8</sup>CSIC, Global Ecology Unit CREAF-CSIC-UAB, Barcelona, Spain.

19 <sup>9</sup>Yellow River Research Institute, North China University of Water Resources and Electric Power,  
20 Zhengzhou 450046, China.

21 <sup>10</sup>Center for Volatile Interactions, University of Copenhagen, Copenhagen, Denmark

## 22 **Corresponding Author**

23 Yongshuo H. Fu ([yfu@bnu.edu.cn](mailto:yfu@bnu.edu.cn))

24 **Spring greening increasing leaf area has strengthened vegetation transpiration**  
25 **and increased the risk of carry-over summer soil moisture depletion across the**  
26 **Northern Hemisphere ( $> 45^\circ \text{ N}$ )<sup>1-4</sup>. The persistence in Autumn and impact on**  
27 **runoff of these effects, however, remain poorly quantified<sup>5,6</sup>. We combined**  
28 **satellite-derived vegetation indices, runoff observations from 297 watersheds,**  
29 **and experiments using the LPJ-GUESS dynamic vegetation model, to**  
30 **demonstrate that spring greening reduced autumnal runoff by an average of**  
31 **1.88-7.34% relative to the baseline from 1982 to 2022, through cross-seasonal**  
32 **carry over effects (CSE) where vegetation growth in one season reduces**  
33 **freshwater availability in subsequent seasons. The CSEs lasted longer in regions**  
34 **dominated by mixed or evergreen forests (until November) than in regions with**  
35 **green vegetation in summer (until October), primarily due to longer foliar**  
36 **longevity. Our findings underscore the need to integrate cross-seasonal**  
37 **interactions between vegetation and hydrology in assessing climate change**  
38 **impacts on water availability and in the planning of sustainable water resources.**  
39 **They also suggest that amplified soil drying in autumn may accelerate the**  
40 **transition of high-latitude ecosystems from carbon sinks to sources.**

41

42 Vegetation regulates the terrestrial balances of water, carbon and energy by mediating  
43 land-atmosphere interactions<sup>7-10</sup>. Climate warming has induced widespread  
44 phenological shifts across the Northern Hemisphere, including earlier spring leaf-out (2.1  
45 d decade<sup>-1</sup>) and delayed autumnal senescence (1.8 d decade<sup>-1</sup>)<sup>5,11,12</sup>, leading to extension  
46 and more intense greening of the growing season. These changes modify water fluxes and the  
47 partitioning of land-surface energy, mostly by enhancing transpiration and interception of  
48 rainfall, with implications for other components of the water balance<sup>13-15</sup>. Crucially, the  
49 resultant shifts in moisture recycling and runoff generation redistribute terrestrial  
50 water resources across time and space, potentially undermining the reliability of  
51 existing water supply systems.

52 Beyond instantaneous effects on evapotranspiration and the interception of rainfall, an  
53 increased leaf area evidenced by vegetation greening can have indirect, cross-seasonal  
54 influences on hydrological processes by depleting soil water and modifying the  
55 ‘memory’ of the land surface (e.g., through legacy effects on soil water and surface  
56 energy partitioning)<sup>16-18</sup>. Observational evidence and model simulations showed that  
57 earlier vegetation growth in spring intensifies summer soil drying by increasing water  
58 consumption before the peak growing season<sup>4,19,20</sup>. Whether such cross-seasonal carry  
59 over effects (CSEs) extend into autumn, however, remains poorly constrained. This  
60 knowledge gap is critical: if early-season greening reduces autumnal runoff (AR), it  
61 could amplify the net loss of carbon dioxide already observed in northern ecosystems  
62 due to autumnal warming<sup>21</sup>, reduce regional fresh water supply<sup>16,20</sup>, and impede  
63 progress toward the Sustainable Development Goals of the United Nations<sup>22</sup>.

64 In this study, we quantified the CSEs of spring and summer vegetation growth on AR  
65 across tundra and boreal ecosystems in the high latitudes (1982-2022) (i.e. based on  
66 RESOLVE Ecoregions 2017<sup>23</sup>). We tested two hypotheses by combining  
67 satellite-derived vegetation indices, runoff observations from 297 watersheds and  
68 factorial simulation experiments using the LPJ-GUESS dynamic vegetation model.  
69 We hypothesize that (1) advanced spring phenology and enhanced summer growth  
70 have a negative legacy effect on AR, and (2) the persistence and intensity of this  
71 effect depend on vegetation type driven by fundamental differences in phenological  
72 strategies and resource allocation between evergreen and deciduous.

### 73 **Seasonal vegetation growth and changes to autumnal runoff**

74 During 1982-2020, satellite observations show a persistent and widespread spring and  
75 summer greening over the study region, while GRUN records show that AR broadly  
76 decreased (Fig. 1a-c,f). The leaf area index (LAI) in spring increased in 68.7% of the  
77 high-latitude areas (mean trend:  $1.68 \pm 0.04 \times 10^{-3} \text{ m}^2 \text{ m}^{-2} \text{ y}^{-1}$ ; Figs. 1a and  
78 Supplementary Fig. 1), with the strongest greening in northern Europe and eastern  
79 Siberia. Independent of wildfire stress, southern Canada exhibited widespread spring  
80 ‘browning’ (predominantly in May), a phenomenon consistent with ‘structural

81 overshoot' wherein precocious resource demand (e.g., for water or nutrients) in early  
82 spring exceeded the ecosystem's immediate carrying capacity, leading to subsequent  
83 browning, (Extended Data Fig. 1c-e and Supplementary Fig. 2), whereas the reduced  
84 summer (June-August) greening rate was associated with the occurrence of wildfires  
85 (Extended Data Fig. 1f-h and 2). Summer greening was even more widespread (65.3%  
86 of the area;  $4.17 \pm 0.14 \times 10^{-3} \text{ m}^2 \text{ m}^{-2} \text{ y}^{-1}$ ), particularly at lower latitudes, with  
87 NDVI-based analyses yielding results consistent with those of LAI (Figs. 1b and  
88 Supplementary Fig. 1).

89 The AR trends were highly spatially heterogeneous, with decreases coinciding with  
90 hotspots of spring greening (Fig. 1). GRUN-based runoff decreased in northern  
91 Europe, eastern and central Canada and parts of Siberia (Fig. 1f), a pattern confirmed  
92 by an independent analysis of 297 minimally disturbed watersheds selected based on  
93 the number of records and the intensity of human activity (see Methods) (Extended  
94 Data Fig. 3). Regions where AR decreased had earlier spring phenologies ( $-0.41 \pm 1.10$   
95  $\text{d decade}^{-1}$  in northern Europe and north-central Siberia) and delayed autumnal  
96 senescence in some areas ( $0.63 \pm 1.28 \text{ d decade}^{-1}$  in southwestern and central Siberia)  
97 (Fig. 1d, e). These regions also had increased precipitation-minus-runoff deficits<sup>17</sup>  
98 across plant functional types (PFTs), indicating that more precipitation was allocated  
99 to other components of the water cycle, such as evapotranspiration (Supplementary  
100 Fig. 3 and 4).

### 101 **Link between seasonal vegetation growth and autumnal runoff**

102 A direct comparison of regions with opposing runoff trends identified distinct  
103 relationships between vegetation and runoff. Areas with reduced AR coincide with a  
104 significantly stronger greening in spring but weaker greening in summer and stronger  
105 browning in autumn than did areas with increased AR (Student's t-test,  $P < 0.05$ ).  
106 Joint probability distributions confirmed that AR was correlated negatively with LAI  
107 trends in spring and autumn but positively with LAI trends in summer (Fig. 1h). To  
108 isolate the effects of vegetation greening (transpiration) from the effects of changes in  
109 precipitation, we analyzed areas where precipitation in autumn remained nearly

110 unchanged ( $<0.1 \text{ mm y}^{-1}$ ). Both LAI- and NDVI-based vegetation greening  
111 consistently reduced AR in these precipitation-stable regions with spring greening  
112 having the strongest CSEs (Extended Data Fig. 4 and Supplementary Fig. 5).

113 A partial-correlation analysis indicated that previous vegetation growth (spring and  
114 summer), rather than concurrent autumnal growth, dominated the vegetation signal in  
115 AR (Fig. 2). After controlling covarying effects of for meteorological factors  
116 (temperature, precipitation, wind speed and shortwave radiation, see Methods), we  
117 found consistent negative correlations between seasonal LAI and AR across the study  
118 region. These associations were substantially stronger for spring (entire region: -0.09;  
119 significant regions ( $P < 0.05$ ): -0.32, the same applies to the subsequent values in  
120 parentheses) and summer (-0.14; -0.40) than for autumn (-0.02; -0.07) (Fig. 2a-f).  
121 This seasonal gradient indicates that the hydrological legacy governing autumnal  
122 runoff is also heavily mediated by summer vegetation growth. As the proximal season  
123 to autumn, enhanced summer greening likely amplifies the initial depletion of soil  
124 water from earlier in the growing season, leading to a cumulative soil water deficit  
125 that ultimately constrains autumnal runoff. Thus, the combined impact of sustained  
126 high water consumption throughout the spring and summer outweighs the direct,  
127 concurrent influence of vegetation activity in autumn.

128 Phenological signals also supported a cross-seasonal mechanism. Spring phenology  
129 (start of the growing season, SOS) was positively correlated with AR (0.09; 0.32), i.e.  
130 earlier spring onset corresponded to lower AR (Fig. 2g, h). In contrast, autumn  
131 phenology (end of the growing season, EOS) was not significantly correlated (Fig. 2i,  
132 j), likely representing counteracting bidirectional feedbacks: delayed senescence  
133 enhanced transpiration and reduced runoff, but water deficits triggered earlier foliar  
134 senescence.

135 The strength and timing of the links between vegetation leaf area and runoff varied  
136 markedly across regions and PFTs. Spring growth (LAI and phenology) had a  
137 stronger influence in northern Europe, whereas summer growth had more influential  
138 in north-central Siberia (Fig. 2a, c, g). Autumnal vegetation had negligible influence

139 throughout the study area. This spatial variability indicated differences in local  
140 climate, soil and vegetation physiology. Notably, spring growth most strongly affected  
141 runoff in regions dominated by evergreen needleleaf forest (ENF; -0.11; -0.34) and  
142 mixed forest (MF; -0.11; -0.32), whereas summer growth had the largest influence in  
143 shrub-dominated regions (SHB; -0.17; -0.43) (Fig. 2k). These PFT-specific patterns  
144 were consistent with differences in the duration of green leaves: ENF and MF  
145 maintained active foliage longer into autumn than did SHB (Extended Data Fig. 5 and  
146 Supplementary Fig. 4,6), extending the window of the influence of vegetation on  
147 hydrological processes.

#### 148 **Cross-seasonal effects on autumnal runoff**

149 By mitigating multicollinearity among predictors, ridge regression identified  
150 divergent temporal signatures of spring and summer vegetation CSEs on AR (see  
151 Methods). Spring LAI had a persistent cross-seasonal negative influence on autumn  
152 runoff, lasting until October across most regions and extending into November in  
153 northern Europe and western Alaska (Fig. 3a-c). In contrast, the effects of summer  
154 LAI were predominantly negative and more pronounced in magnitude but exhibited  
155 lower persistence; these suppressive impacts peaked in September, with only sporadic  
156 instances extending into October (Fig. 3e-g). The magnitude and duration of the CSEs  
157 were decoupled: the spring effects lasted longer, but their per-unit impact on runoff  
158 was not necessarily stronger than the summer effects, a pattern consistently observed  
159 in the NDVI-based analysis (Fig. 3d, h and Supplementary Fig. 7d, h).

160 The persistence of the CSEs, defined as the temporal window preceding a sharp  
161 decline in influence compared to the previous month, varied strongly across  
162 vegetation types. Broadleaf vegetation had a larger impact on AR in spring before  
163 canopy closure (before the peak of the season, POS) (Fig. 3d), likely due to rapid  
164 early-season leaf expansion and high transpiration rates that draw down soil water  
165 stores. The differences between the vegetation types decreased in summer, after LAI  
166 saturation (POS), with all PFTs having significant but transient effects (Fig. 3h).  
167 Notably, SHB (-11.47 mm per unit LAI) was the PFT with the strongest CSEs of

168 spring growth, and MF and ENF (to November) were the PFTs with the most  
169 persistent CSEs.

170 The factorial experiments that used the LPJ-GUESS model independently  
171 corroborated these patterns (by controlling the spring phenology, see Methods). The  
172 model, forced by CRUNCEP v7 climate data, accurately reproduced the observed  
173 variations (90%) in AR (Supplementary Fig. 8). Scenario experiments isolating the  
174 effects of spring phenology confirmed that early-season vegetation growth decreased  
175 AR by  $-5.25 \pm 0.05$  mm per unit LAI, Extended Data Fig. 6 and Supplementary 9),  
176 with the CSEs weakening from September (-5.05%) to November (-0.40%) (Fig. 4). A  
177 consistent spatial weakening of CSEs from September to November is evident in both  
178 model simulations and observations (Extended Data Fig. 7). MF and ENF had the  
179 most persistent CSEs, likely indicating sustained but reduced physiological activity in  
180 autumn (Extended Data Fig. 10), consistent with the observational analysis. The CSEs  
181 in areas with deciduous needleleaf forest (DNF) were mostly confined to September;  
182 the effects in areas dominated by DBF and SHB peaked in October.

183 Based on the convergence of the observational evidence and the model experiments,  
184 we extended the same modeling framework to 1982-2022 to assess whether the CSEs  
185 had intensified in recent decades. The simulations identified consistent patterns and  
186 indicated a stronger CSEs (1.88-7.34% reduction, signifying an enhanced persistence)  
187 of 1982-2022 than that of 1982-2014 (Extended Data Fig. 8). Notably, the November  
188 CSEs was markedly higher for DBF than for other vegetation types, which might be  
189 attributed to biases caused by the limited coverage of DBF in the northern  
190 hemisphere.

191 A conceptual integration reveals that divergent phenological trajectories dictate the  
192 characteristic duration of CSEs across distinct plant functional types (PFTs). Spring  
193 greening intensified summer growth in PFT-dominated regions that are green in  
194 summer (Fig. 5a), increasing water demand before autumn and potentially  
195 exacerbating deficits of soil water (Extended Data Fig. 9). Rapid autumnal senescence,  
196 however, reduced the direct influence of vegetation on hydrological processes. In

197 contrast, persistent green foliage in regions with mixed or evergreen forest (Fig. 5b)  
198 extended the window of the coupling between vegetation and hydrology into late  
199 autumn, by both direct transpiration and modification of land-surface properties, even  
200 under environmental stress. This phenological divergence reconciles the PFT-specific  
201 persistence of CSEs observed across scales, identifying biological senescence  
202 trajectories as a primary determinant of cross-seasonal hydrological memory.

### 203 **Discussion**

204 Through analyses of satellite greening trends, watershed-scale runoff data and  
205 process-based model experiments, we provide evidence that spring greening can  
206 reduce AR across ecosystems at high latitudes by a CSE. The magnitude of this  
207 reduction (1.88-7.34% from 1982 to 2022) and its persistence extending into  
208 November in mixed and evergreen forests, indicated a previously underappreciated  
209 dimension of the coupling between vegetation and hydrology. The  
210 vegetation-mediated depletion of soil water is the mechanism underlying the  
211 CSEs. Enhanced spring and summer transpiration, driven by increased leaf area and  
212 earlier onset of the growing season, reduces the storage of soil water (Extended Data  
213 Fig. 9) that would otherwise sustain autumn baseflow<sup>4,19,24</sup>. This CSE is  
214 PFT-dependent: the hydrological influence in ecosystems with prolonged foliar  
215 activity (MF and ENF) persists longer because green leaves continue to extract soil  
216 water and modify surface fluxes even as autumn progresses. In contrast, PFTs that  
217 remain green in summer (DBF and SHB) rapidly decouple from hydrological  
218 processes following senescence, limiting their influence only to early autumn.

219 These findings have implications for both water resources and the carbon  
220 cycle. Reduced AR implies a lower availability of freshwater during a season critical  
221 for ecosystem recharge and, in some regions, anthropogenic water use<sup>25</sup>. More  
222 importantly, the accompanying soil drying may amplify the net loss of carbon dioxide  
223 associated with autumnal warming<sup>21</sup>. Northern ecosystems currently act as carbon  
224 sinks, but warming-induced increases in respiration already threaten this status<sup>26</sup>. Our  
225 results suggest that the vegetation-driven depletion of soil water could further tip the

226 balance toward carbon source behavior by inducing drought stress that suppresses  
227 photosynthesis while heterotrophic respiration continues<sup>27</sup>. The stronger CSEs in  
228 mixed and evergreen forests the ecosystems with the largest carbon stores, increases  
229 this concern.

230 The strengthening of CSEs in autumn over recent decades (Extended Data Fig. 8)  
231 raises concerns about future of water availability in autumn. Continued warming is  
232 expected to further advance spring phenology and enhance greening<sup>5,11</sup>, potentially  
233 amplifying cross-seasonal hydrological effects. The response, however, may be  
234 nonlinear: if warming-induced drought stress becomes severe enough to trigger  
235 ‘structural overshoot’ (as observed in parts of southern Canada; Extended Data Fig.  
236 2-4) or widespread mortality, the CSEs could decrease<sup>28,29</sup>. The contrasting behaviors  
237 of the PFTs also suggest that climatically driven shifts in vegetation, e.g. expansion of  
238 shrubs into tundra or changes in forest composition, could alter regional hydrological  
239 patterns in ways not identified by current models<sup>30-34</sup>.

240 The following limitations of our analysis should be acknowledged. The observational  
241 record for long-term trend detection is relatively short, and its coarse spatial  
242 resolution may obscure fine-scale hydrological processes. While mechanistically  
243 grounded, the LPJ-GUESS simulations lack explicit representation of lateral  
244 subsurface flow and groundwater dynamics, which can modulate CSEs in complex  
245 terrain. Regarding the drivers of browning, although we emphasize structural  
246 overshoot, recurrent wildfires, particularly in high-latitude North America, may  
247 decouple LAI-based mechanisms from hydrological responses by altering post-fire  
248 runoff independently of phenology<sup>35,36</sup>. This factor might introduce additional  
249 variability not captured by phenological metrics, potentially influencing the  
250 magnitude or spatial pattern of the observed CSEs. Furthermore, uncertainties may  
251 arise from inconsistent vegetation trends across different satellite sensors and leaf area  
252 index (LAI) products. While our findings are robust across multiple datasets, the  
253 inherent discrepancies in sensor calibration and retrieval algorithms introduce a  
254 degree of quantitative uncertainty in the estimated magnitudes of greening and its

255 subsequent hydrological impacts. Additionally, high seasonal autocorrelation hinders  
256 the complete isolation of individual seasonal effects; while our scenario experiments  
257 mitigate this, synergistic impacts may persist. uncertainties in plant functional type  
258 (PFT) classifications or dynamic shifts in PFT distribution over the study period could  
259 introduce complexities in interpreting PFT-specific responses. These constraints  
260 define priorities for future research.

261 Enhancing the integration of vegetation dynamics into hydrological models,  
262 specifically PFT-specific phenology and transpiration, is essential. Next-generation  
263 Earth system models must incorporate cross-seasonal vegetation-water coupling to  
264 improve predictions of water availability and carbon-cycle feedbacks<sup>37,38</sup>. Finally,  
265 high-resolution remote sensing of vegetation water status and soil water, integrated  
266 with dense in situ networks, will provide the observational constraints necessary to  
267 refine these mechanistic underpinnings.

268 In conclusion, our results established that spring greening reduced AR across high  
269 latitudes by a CSE, whose duration depended on vegetation type. This coupling  
270 between seasonal vegetation growth and hydrological processes represents an  
271 important climatic feedback that couples the water and carbon cycles, with  
272 implications for water security, ecosystem function and policy for mitigating climate  
273 change.

274 **Methods**

275 **Remotely sensed and reanalysis data sets**

276 We investigated the impact of seasonal vegetation growth on variations of autumnal  
277 runoff (AR) at high latitudes in the Northern Hemisphere using the GRUN gridded  
278 runoff reconstruction data set across 1982-2014. The data set was trained and  
279 cross-validated using data for observed stream flow with high accuracy and low  
280 uncertainty<sup>39</sup>. The Climatic Research Unit-National Centers for Environmental  
281 Prediction (CRUNCEP) v7 data for monthly climate, spanning 1982-2014 (consistent  
282 with the GRUN dataset), has a horizontal resolution of  $0.5 \times 0.5^\circ$  and are a  
283 combination of CRU TS3.2 and NCEP reanalysis data, including air temperature,  
284 precipitation, humidity, wind speed, number of wet days, and amount of incoming  
285 solar radiation<sup>40</sup>. The CRU JRA data set is a blend of CRU and JRA data sets with the  
286 same spatial resolution as the CRUNCEP data set, but with longer records  
287 (1901-2022)<sup>41</sup>. We used the Global Inventory Modeling and Mapping Studies 4th  
288 Generation (GIMMS4g) data set for leaf area index (LAI) to identify seasonal  
289 vegetation growth dynamics. This long-term dataset, spanning 1982-2020, minimizes  
290 effects of satellite orbital drift and sensor degradation, and has demonstrated superior  
291 performance across most vegetation biomes, with LAI derived using a  
292 back-propagation neural network<sup>42</sup>. The data set for vegetation phenology, i.e. SOS  
293 (EOS), the start (end) of the growing season, was obtained by integrating five  
294 methods of phenological extraction and has the same source data as GIMMS<sub>4g</sub> LAI<sup>43</sup>.  
295 The Advanced Very High Resolution Radiometer (AVHRR) NDVI was employed to  
296 characterize long-term (1982-2020) vegetation greenness, specifically leveraging a  
297 refined global dataset with improved consistency across sensor transitions<sup>44</sup>. To  
298 account for the impacts of fire disturbances, we utilized the FireCCILT11 long-term  
299 burned area dataset, spanning 1982-2014, which provides multi-sensor integrated  
300 records of wildfire occurrences optimized for historical trend analysis<sup>45</sup>. All datasets  
301 were resampled to a  $0.5^\circ \times 0.5^\circ$  resolution using nearest-neighbor interpolation. The  
302 temporal span of each analysis was determined by the shortest record length among

303 the constituent datasets: analyses involving GRUN covered 1982-2014, whereas those  
304 based on LPJ-GUESS simulations could be extended from 1982 to 2022. We  
305 investigated the effects of seasonal vegetation growth on AR in different  
306 PFT-dominated regions using the Global Land Cover (GLC) 2000 data set for  
307 land-cover type at a resolution of 1 km, which combines satellite imagery and ground  
308 surveys<sup>46</sup>. The proportion of each land-cover type in the range of 0.5×0.5° was  
309 calculated, and the type with the largest proportion was defined as the dominant type.

310 The data set from the Global Runoff Data Centre (GRDC, <https://grdc.bafg.de/>) was  
311 used to identify the trend of AR at the catchment scale and ensure spatial consistency  
312 between gridded-runoff and in situ records. A total of 297 catchments (Extended Data  
313 Fig. 3) were selected based on two criteria: 1) containing at least 10 years of  
314 observational records from 1982 to 2014, and 2) eliminating the influence of  
315 anthropogenic activities (e.g. irrigation and water withdrawal by urban residents) on  
316 hydrological processes. Catchments with irrigated areas >3% and urban areas >1%  
317 were excluded based on the Global Map of Irrigation Areas and GLC2000 land  
318 cover<sup>46-48</sup>.

### 319 **Impacts and their duration of seasonal vegetation growth on autumnal runoff**

320 Changes in AR are affected not only by meteorological factors of the season, but also  
321 to a large extent by the state of the underlying surface in previous seasons, especially  
322 the dynamics of vegetation growth. We separated the effects of each common  
323 influencing factor to reduce bias using a partial-correlation analysis to explore the  
324 relationship between seasonal vegetation growth/meteorological factors and AR<sup>49</sup>.  
325 Seasonal vegetation growth included LAI in spring, summer and autumn and spring  
326 and autumnal phenologies, which characterize the time and state of vegetation growth;  
327 meteorological factors included temperature, precipitation, wind speed and amount of  
328 incoming shortwave radiation in the season<sup>9,20</sup>.

329 The seasonal growth of vegetation is highly consistent with the seasonal fluctuation of  
330 the hydrological cycle within a year. The state of the growth of vegetation in the  
331 previous season will affect the hydrological cycle in the current season by the CSE<sup>4,24</sup>.

332 The regularized linear regression model (ridge regression) was used to quantify the  
 333 relationship between vegetation growth in spring and summer with autumnal  
 334 (September-November) runoff, thereby identifying the magnitude of the CSE of  
 335 seasonal vegetation growth on AR (Eq. 1). Ridge regression is a standard technique  
 336 for estimating the coefficients of strongly correlated independent variables, such as  
 337 seasonal vegetation growth. A ridge-regression regularization parameter is created,  
 338 and the regression coefficients are decreased to obtain more-accurate estimates of the  
 339 ridge parameters<sup>50-52</sup>, where the goal is to minimize the loss function given by the  
 340 residual sum of squares (*RSS*, Eq. 2).

$$Runoff = \sum_{i=1}^n X_i \beta_i + \beta_0 + \varepsilon \quad (\text{Eq. 1})$$

$$RSS = \sum_{j=1}^{years} (Runoff_j - X_j^T \beta) = \|Runoff - X \beta\|_2^2 \quad (\text{Eq. 2})$$

341 where the subscript *i* represents the number of variables,  $\beta$  is the regression coefficient  
 342 and the subscript *j* represents the value of each year, i.e. 1982 to 2014. The penalty  
 343 term based on the  $L_2$  norm, i.e. the sum of squared coefficients and the regularization  
 344 parameter  $\lambda$ , is introduced to balance the trade-off between bias and variance, as in the  
 345 Eq. 3:

$$\hat{\beta} = \arg \min_{\beta} \left[ RSS + \lambda \|\beta\|_2^2 \right] \quad (\text{Eq. 3})$$

### 346 **LPJ-GUESS model experiments**

347 LPJ-GUESS is a process-based dynamic global vegetation model (DGVM) that  
 348 simulates vegetation structural and compositional successions, including phenological  
 349 shifts, alongside the coupled terrestrial fluxes of carbon, nitrogen, phosphorus, and  
 350 water within each grid cell<sup>53-55</sup>. Each grid cell consists of multiple stand types,  
 351 representing the land use of that grid, and each stand simulates multiple patches  
 352 (approximately the maximum area of influence of an adult plant on its neighbors),

353 representing different disturbance histories of the stands, and the simulated properties  
354 generally converge to a single, comprehensive average value<sup>31,56</sup>. LPJ-GUESS  
355 provides a detailed description of the processes of vegetation growth, including the  
356 responses of vegetation to environmental factors and to competition among plants for  
357 resources such as nutrients, light and space, and of hydrological processes such as  
358 interception, infiltration and transpiration<sup>57</sup>. LPJ-GUESS is an advanced modeling  
359 approach for simulating seasonal vegetation growth and its impact on the water cycle.

360 To isolate the cross-seasonal effects, we designed two LPJ-GUESS simulations. In  
361 the control simulation, spring phenology was allowed to vary naturally according to  
362 observed climatic conditions. In the experimental simulation, the spring phenology  
363 module was modified to remove the long-term trend in SOS. Specifically, the start  
364 time of the growing season (SOS) was fixed to a constant average timing derived  
365 from the initial five years of the control simulation (1982-1986 average  
366 temperature-driven SOS) for the entire 1982-2022 simulation period (Extended Data  
367 Fig. 6). This allowed us to isolate the hydrological impact of the observed trend  
368 towards earlier spring phenology by comparing it against a scenario without such  
369 advancement. This approach ensures that any differences in autumnal runoff between  
370 the two simulations are attributable solely to the long-term changes and interannual  
371 variability in spring phenology and subsequent vegetation growth that occurred in the  
372 control run, excluding the impact of phenological trends. We conducted two  
373 simulations with the same inputs and settings except for the module for spring  
374 phenology. To drive the LPJ-GUESS simulations, we employed CRUNCEP v7  
375 climatic data (0.5°×0.5° resolution) for the 1901-2014 period, which supported the  
376 initial 500-year spin-up and the historical simulation. To extend our analysis to the  
377 1982-2022 study period, we transitioned to the CRU JRA dataset, ensuring temporal  
378 continuity and consistency across all analyses. The model state, including soil carbon  
379 and nitrogen pools and water balance components, was archived at the end of 1981 after  
380 the spin-up and historical transient run; this saved state served as the standardized  
381 baseline for the 1982-2022 simulations, thereby eliminating potential discrepancies in

382 initial ecosystem conditions. The second step was to restart two simulation scenarios  
383 using the saved system state, one forced by actual climatic conditions and the other  
384 simulated with the same forcing but controlling spring phenology (Extended Data Fig.  
385 10). The difference in autumnal monthly runoff between the two simulation scenarios  
386 is caused by the difference in early vegetation growth (SOS, spring LAI and summer  
387 LAI), and the percentage of this difference compared to the control can be quantified  
388 using the Eq. 4:

$$Diff_m^{growth} = \frac{Runoff_m^{control} - Runoff_m^{contrast}}{Runoff_m^{contrast}} \times 100\% \quad m \in \{9, 10, 11\} \quad (\text{Eq. 4})$$

389

390 **Data availability**

391 All data used in this study are accompanied by corresponding sources and references,  
392 which are detailed in the relevant sections of the paper, and the source codes for the  
393 LPJ-GUESS model, data interpretation and figure preparation are available from the  
394 corresponding author upon request.

395 **Competing Interest**

396 The authors declare no known competing financial interests or personal relationships  
397 that influenced the work reported in this paper.

398 **Author contributions**

399 Y.H.F. formulated the original concept presented in the paper. Y.H.F., S.Z.C. and J.T.  
400 contributed to discussions regarding the study design. J.T. guided the LPJ-GUESS  
401 model experiments setup and S.Z.C. modified the LPJ-GUESS model and conducted  
402 all statistical analyses. S.Z.C. and Y.H.F. authored the initial draft of the paper. All  
403 authors engaged in the discussion and revision processes of the paper.

404 **Acknowledgements**

405 Y.H.F. is supported by the National Science Fund for the Key Program of the National  
406 Natural Science Foundation of China (42430504) and National key research and  
407 development program (2023YFF0805604) and the work was supported by the  
408 International Cooperation and Exchanges NSFC-STINT (42111530181), J.T. is  
409 supported by Villum Young Investigator (Grant number VIL53048), Swedish  
410 FORMAS (Forskningsråd för hållbar utveckling) mobility Grant (2016-01580), Lund  
411 University strategic research area MERGE and European Union's Horizon 2020  
412 research and innovation programme under Marie Skłodowska-Curie (Grant 707187)  
413 and ERC consolidator grant (TUVOLU, Grant number 771012). J.T. acknowledge the  
414 support by the Danish National Research Foundation within the Center for Volatile  
415 Interactions (VOLT, DNRF168). S.Z.C., J.T. and Y.H.F. thank the Joint China-Sweden  
416 Mobility Program (Grant number CH2020-8656). This study was supported by the

417 111 Project (B18006). JP acknowledges support from the grant CONCERTO (Grant  
418 Agreement 101185000, HORIZON-CL5-2024-D1-01, European Union). M.F-M was  
419 supported by the European Research Council project ERC-StG-2022-101076740  
420 STOIKOS, and by a Ramón y Cajal fellowship (RYC2021-031511-I) funded by the  
421 Spanish Ministry of Science and Innovation, the NextGenerationEU program of the  
422 European Union, the Spanish plan of recovery, transformation and resilience, and the  
423 Spanish Research Agency.

424 **Reference**

- 425 1 Zeng, Z., Peng, L. & Piao, S. Response of terrestrial evapotranspiration to Earth's greening.  
426 *Current Opinion in Environmental Sustainability* **33**, 9-25 (2018).
- 427 2 Yang, Y. *et al.* Evapotranspiration on a greening Earth. *Nature Reviews Earth & Environment* **4**,  
428 626-641 (2023).
- 429 3 Piao, S. *et al.* Characteristics, drivers and feedbacks of global greening. *Nature Reviews Earth &*  
430 *Environment* **1**, 14-27 (2020).
- 431 4 Lian, X. *et al.* Summer soil drying exacerbated by earlier spring greening of northern vegetation.  
432 *Science Advances* **6**, eaax0255, doi:doi:10.1126/sciadv.aax0255 (2020).
- 433 5 Piao, S. *et al.* Plant phenology and global climate change: Current progresses and challenges.  
434 *Global Change Biology* **25**, 1922-1940, doi:<https://doi.org/10.1111/gcb.14619> (2019).
- 435 6 Peñuelas, J., Rutishauser, T. & Filella, I. Phenology feedbacks on climate change. *Science* **324**,  
436 887-888 (2009).
- 437 7 Bonan, G. B. Forests and Climate Change: Forcings, Feedbacks, and the Climate Benefits of  
438 Forests. *Science* **320**, 1444-1449, doi:doi:10.1126/science.1155121 (2008).
- 439 8 Cui, J. *et al.* Global water availability boosted by vegetation-driven changes in atmospheric  
440 moisture transport. *Nature Geoscience* **15**, 982-988, doi:10.1038/s41561-022-01061-7 (2022).
- 441 9 Chen, S. *et al.* Vegetation phenology and its ecohydrological implications from individual to  
442 global scales. *Geography and Sustainability* **3**, 334-338 (2022).
- 443 10 Bonan, G. B., Pollard, D. & Thompson, S. L. Effects of boreal forest vegetation on global climate.  
444 *Nature* **359**, 716-718, doi:10.1038/359716a0 (1992).
- 445 11 Zhu, Z. *et al.* Greening of the Earth and its drivers. *Nature climate change* **6**, 791-795 (2016).
- 446 12 Keenan, T. F. *et al.* Net carbon uptake has increased through warming-induced changes in  
447 temperate forest phenology. *Nature Climate Change* **4**, 598-604, doi:10.1038/nclimate2253  
448 (2014).
- 449 13 Bonan, G. B. Forests, Climate, and Public Policy: A 500-Year Interdisciplinary Odyssey. *Annual*  
450 *Review of Ecology, Evolution, and Systematics* **47**, 97-121,  
451 doi:<https://doi.org/10.1146/annurev-ecolsys-121415-032359> (2016).
- 452 14 Davin, E. L. & de Noblet-Ducoudré, N. Climatic Impact of Global-Scale Deforestation: Radiative  
453 versus Nonradiative Processes. *Journal of Climate* **23**, 97-112,  
454 doi:<https://doi.org/10.1175/2009JCLI3102.1> (2010).
- 455 15 Piao, S. *et al.* Characteristics, drivers and feedbacks of global greening. *Nature Reviews Earth &*  
456 *Environment* **1**, 14-27, doi:10.1038/s43017-019-0001-x (2020).
- 457 16 Hwang, T., Band, L. E., Oishi, A. C. & Kang, H. Greenup Variability Impact on Seasonal  
458 Streamflow and Soil Moisture Dynamics in Humid, Temperate Forests. *Water Resources Research*  
459 **59**, e2022WR034125, doi:<https://doi.org/10.1029/2022WR034125> (2023).
- 460 17 Hwang, T. *et al.* Nonstationary Hydrologic Behavior in Forested Watersheds Is Mediated by  
461 Climate-Induced Changes in Growing Season Length and Subsequent Vegetation Growth. *Water*  
462 *Resources Research* **54**, 5359-5375, doi:<https://doi.org/10.1029/2017WR022279> (2018).
- 463 18 Kim, J. H. *et al.* Warming-Induced Earlier Greenup Leads to Reduced Stream Discharge in a  
464 Temperate Mixed Forest Catchment. *Journal of Geophysical Research: Biogeosciences* **123**,  
465 1960-1975, doi:<https://doi.org/10.1029/2018JG004438> (2018).
- 466 19 Evaristo, J. & McDonnell, J. J. Global analysis of streamflow response to forest management.  
467 *Nature* **570**, 455-461, doi:10.1038/s41586-019-1306-0 (2019).

- 468 20 Geng, X. *et al.* Extended growing season reduced river runoff in Luanhe River basin. *Journal of*  
469 *Hydrology* **582**, 124538 (2020).
- 470 21 Piao, S. *et al.* Net carbon dioxide losses of northern ecosystems in response to autumn warming.  
471 *Nature* **451**, 49-52, doi:10.1038/nature06444 (2008).
- 472 22 Soergel, B. *et al.* A sustainable development pathway for climate action within the UN 2030  
473 Agenda. *Nature Climate Change* **11**, 656-664, doi:10.1038/s41558-021-01098-3 (2021).
- 474 23 Dinerstein, E. *et al.* An ecoregion-based approach to protecting half the terrestrial realm.  
475 *BioScience* **67**, 534-545 (2017).
- 476 24 Lian, X. *et al.* Diminishing carryover benefits of earlier spring vegetation growth. *Nature Ecology*  
477 *& Evolution* **8**, 218-228, doi:10.1038/s41559-023-02272-w (2024).
- 478 25 Kan, F. *et al.* Latitudinal divergence in runoff responses to global forestation due to  
479 forest-atmosphere feedbacks. *Nature Communications*, doi:10.1038/s41467-026-68945-9 (2026).
- 480 26 Martínez-García, E. *et al.* Drought response of the boreal forest carbon sink is driven by  
481 understorey–tree composition. *Nature Geoscience* **17**, 197-204, doi:10.1038/s41561-024-01374-9  
482 (2024).
- 483 27 McDowell, N. G. *et al.* Pervasive shifts in forest dynamics in a changing world. *Science* **368**,  
484 eaaz9463, doi:doi:10.1126/science.aaz9463 (2020).
- 485 28 Buermann, W. *et al.* Recent shift in Eurasian boreal forest greening response may be associated  
486 with warmer and drier summers. *Geophysical Research Letters* **41**, 1995-2002,  
487 doi:<https://doi.org/10.1002/2014GL059450> (2014).
- 488 29 Li, Y. *et al.* Widespread spring phenology effects on drought recovery of Northern Hemisphere  
489 ecosystems. *Nature Climate Change* **13**, 182-188, doi:10.1038/s41558-022-01584-2 (2023).
- 490 30 Mashwani, Z.-u.-R. Environment, climate change and biodiversity. *Environment, climate, plant*  
491 *and vegetation growth*, 473-501 (2020).
- 492 31 Chen, S. *et al.* A new temperature–photoperiod coupled phenology module in LPJ-GUESS model  
493 v4.1: optimizing estimation of terrestrial carbon and water processes. *Geosci. Model Dev.* **17**,  
494 2509-2523, doi:10.5194/gmd-17-2509-2024 (2024).
- 495 32 Huang, M. *et al.* Air temperature optima of vegetation productivity across global biomes. *Nature*  
496 *Ecology & Evolution* **3**, 772-779, doi:10.1038/s41559-019-0838-x (2019).
- 497 33 Fu, Y. H. *et al.* Declining global warming effects on the phenology of spring leaf unfolding.  
498 *Nature* **526**, 104-107, doi:10.1038/nature15402 (2015).
- 499 34 Xi, Y., Zhang, W., Wei, F., Fang, Z. & Fensholt, R. Boreal tree species diversity increases with  
500 global warming but is reversed by extremes. *Nature Plants* **10**, 1473-1483,  
501 doi:10.1038/s41477-024-01794-w (2024).
- 502 35 Goetz, S. J., Mack, M. C., Gurney, K. R., Randerson, J. T. & Houghton, R. A. Ecosystem  
503 responses to recent climate change and fire disturbance at northern high latitudes: observations  
504 and model results contrasting northern Eurasia and North America. *Environmental Research*  
505 *Letters* **2**, 045031, doi:10.1088/1748-9326/2/4/045031 (2007).
- 506 36 Partington, D. *et al.* Predicting wildfire induced changes to runoff: A review and synthesis of  
507 modeling approaches. *WIREs Water* **9**, e1599, doi:<https://doi.org/10.1002/wat2.1599> (2022).
- 508 37 Chen, M. *et al.* Iterative integration of deep learning in hybrid Earth surface system modelling.  
509 *Nature Reviews Earth & Environment* **4**, 568-581, doi:10.1038/s43017-023-00452-7 (2023).
- 510 38 Fu, Y. *et al.* Progress in plant phenology modeling under global climate change. *Science China*  
511 *Earth Sciences* **63**, 1237-1247, doi:10.1007/s11430-019-9622-2 (2020).

512 39 Ghiggi, G., Humphrey, V., Seneviratne, S. I. & Gudmundsson, L. GRUN: an observation-based  
513 global gridded runoff dataset from 1902 to 2014. *Earth Syst. Sci. Data* **11**, 1655-1674,  
514 doi:10.5194/essd-11-1655-2019 (2019).

515 40 Viovy, N. CRUNCEP version 7-atmospheric forcing data for the community land model. *Research*  
516 *Data Archive at the National Center for Atmospheric Research, Computational and Information*  
517 *Systems Laboratory* **10** (2018).

518 41 Harris, I. C. CRU JRA v2.4: A forcings dataset of gridded land surface blend of Climatic Research  
519 Unit (CRU) and Japanese reanalysis (JRA) data. (2023).

520 42 Cao, S. *et al.* Spatiotemporally consistent global dataset of the GIMMS leaf area index (GIMMS  
521 LAI4g) from 1982 to 2020. *Earth Syst. Sci. Data* **15**, 4877-4899, doi:10.5194/essd-15-4877-2023  
522 (2023).

523 43 Shouzhi, C. & yongshuo, F. Vegetation phenology data based on GIMMS4g NDVI from 1982 to  
524 2020. doi:10.5281/zenodo.11136967 (2024).

525 44 Jeong, S. *et al.* Persistent global greening over the last four decades using novel long-term  
526 vegetation index data with enhanced temporal consistency. *Remote Sensing of Environment* **311**,  
527 114282, doi:<https://doi.org/10.1016/j.rse.2024.114282> (2024).

528 45 Otón, G., Lizundia-Loiola, J., Pettinari, M. L. & Chuvieco, E. Development of a consistent global  
529 long-term burned area product (1982–2018) based on AVHRR-LTDR data. *International Journal*  
530 *of Applied Earth Observation and Geoinformation* **103**, 102473,  
531 doi:<https://doi.org/10.1016/j.jag.2021.102473> (2021).

532 46 Bartholomé, E. & Belward, A. S. GLC2000: a new approach to global land cover mapping from  
533 Earth observation data. *International Journal of Remote Sensing* **26**, 1959-1977,  
534 doi:10.1080/01431160412331291297 (2005).

535 47 Han, J. *et al.* Streamflow seasonality in a snow-dwindling world. *Nature* **629**, 1075-1081,  
536 doi:10.1038/s41586-024-07299-y (2024).

537 48 Siebert, S. *et al.* A global data set of the extent of irrigated land from 1900 to 2005. *Hydrol. Earth*  
538 *Syst. Sci.* **19**, 1521-1545, doi:10.5194/hess-19-1521-2015 (2015).

539 49 Mardia, K. V., Kent, J. T. & Taylor, C. C. *Multivariate analysis*. Vol. 88 (Academic Press, 1979).

540 50 McDonald, G. C. Ridge regression. *Wiley Interdisciplinary Reviews: Computational Statistics* **1**,  
541 93-100 (2009).

542 51 Sippel, S. *et al.* Robust detection of forced warming in the presence of potentially large climate  
543 variability. *Science Advances* **7**, eabh4429, doi:doi:10.1126/sciadv.abh4429 (2021).

544 52 Sippel, S., Meinshausen, N., Fischer, E. M., Székely, E. & Knutti, R. Climate change now  
545 detectable from any single day of weather at global scale. *Nature Climate Change* **10**, 35-41,  
546 doi:10.1038/s41558-019-0666-7 (2020).

547 53 Sitch, S. *et al.* Evaluation of ecosystem dynamics, plant geography and terrestrial carbon cycling  
548 in the LPJ dynamic global vegetation model. *Global change biology* **9**, 161-185 (2003).

549 54 Morales, P. *et al.* Comparing and evaluating process-based ecosystem model predictions of carbon  
550 and water fluxes in major European forest biomes. *Global change biology* **11**, 2211-2233 (2005).

551 55 Hickler, T. *et al.* Using a generalized vegetation model to simulate vegetation dynamics in  
552 northeastern USA. *Ecology* **85**, 519-530 (2004).

553 56 Smith, B. LPJ-GUESS-an ecosystem modelling framework. *Department of Physical Geography*  
554 *and Ecosystems Analysis, INES, Sölvegatan* **12**, 22362 (2001).

555 57 Tang, J., Miller, P. A., Crill, P. M., Olin, S. & Pilesjö, P. Investigating the influence of two  
556 different flow routing algorithms on soil–water–vegetation interactions using the dynamic  
557 ecosystem model LPJ-GUESS. *Ecohydrology* **8**, 570-583, doi:<https://doi.org/10.1002/eco.1526>  
558 (2015).  
559  
560

561 **Figure legends**

562 **Figure 1. Patterns of spatiotemporal variations of seasonal vegetation growth**  
563 **and autumnal runoff during 1982-2014.** (a-f) Spatiotemporal variations of (a)  
564 spring LAI, (b) summer LAI, (c) autumnal LAI, (d) start of the growing season, (e)  
565 end of the growing season and (f) autumnal runoff (AR). For each of the graphs in  
566 (a-f), the bottom-left histogram (units as in the color scale) represents the data  
567 distribution, the dashed lines represent means and the regions marked by slashes  
568 indicate significant changes (linear regression,  $P < 0.05$ ). (g) Trends of changes in  
569 seasonal vegetation growth and AR in regions with decreased and increased AR,  
570 respectively. (h) The joint distributions of the trends of seasonal vegetation growth  
571 ( $\text{m}^2 \text{m}^{-2} \text{y}^{-1}$ ) and AR ( $\text{mm y}^{-1}$ ). The greener the color, the denser the data. The solid  
572 black lines represent the linear fits between the trends of AR and vegetation growth in  
573 different seasons.

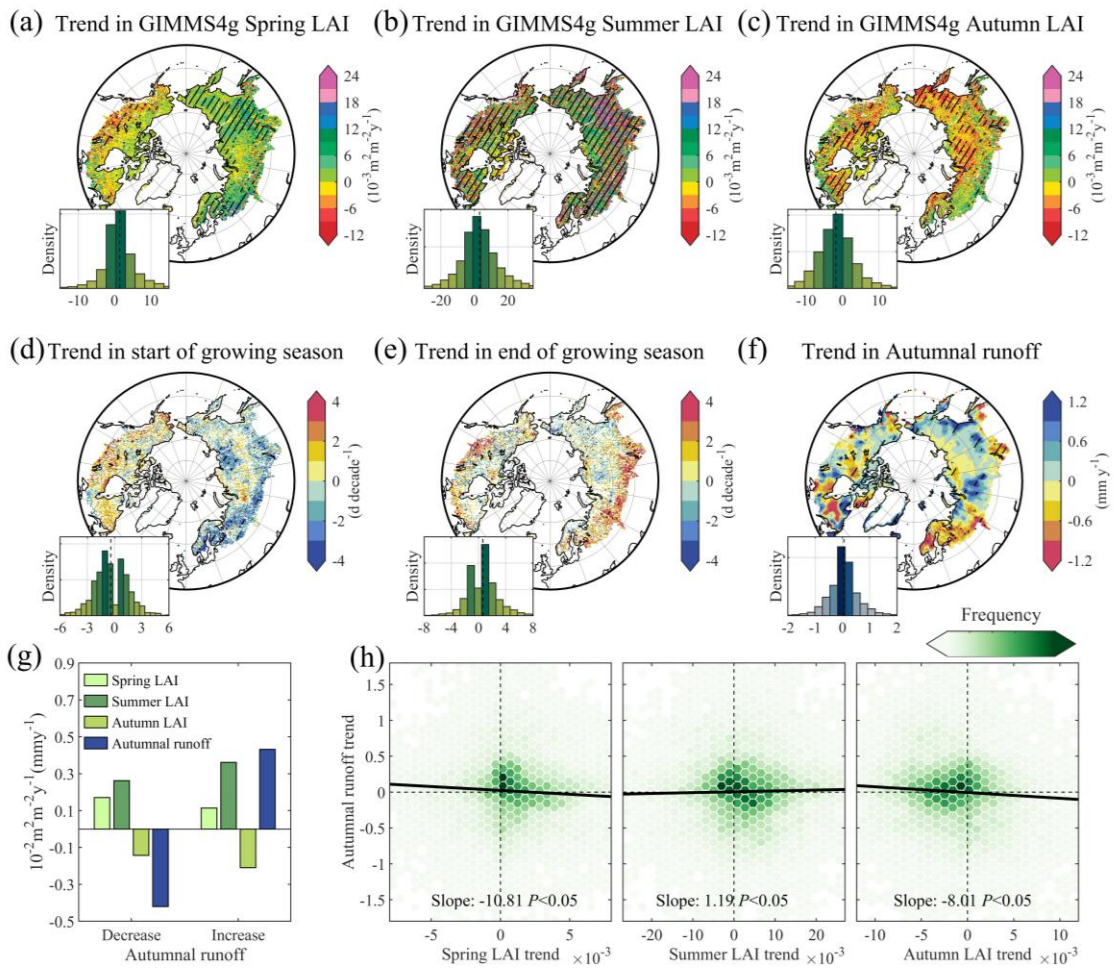
574 **Figure 2. Partial correlations between seasonal vegetation growth (leaf area**  
575 **index and vegetation phenology) and autumnal runoff.** (a, c, e, g and i) Spatial  
576 patterns of partial-correlation coefficients between (a) spring LAI, (c) summer LAI, (e)  
577 autumnal LAI, (g) start of the growing season (SOS) (i) end of the growing season  
578 (EOS) and autumnal runoff, respectively. The meteorological factors, i.e. temperature,  
579 precipitation, wind speed, and incoming shortwave radiation, were included in the  
580 analysis to exclude their influence. The regions marked by slashes indicate significant  
581 correlations ( $P < 0.05$ ). (b, d, f, h and j) Frequency distributions of the  
582 partial-correlation coefficients between (b) spring LAI, (d) summer LAI, (f) autumnal  
583 LAI, (h) SOS and (j) EOS and autumnal runoff across the plant functional types,  
584 respectively. (k) Mean partial-correlation coefficients between seasonal vegetation  
585 growth and autumnal runoff across the plant functional types. Dark bars represent all  
586 regions, and light bars represent regions with significant correlations. ALL, all PFTs;  
587 SHB, shrub; MF, mixed forest; DNF, deciduous needle-leaved forest; ENF, evergreen  
588 needle-leaved forest; DBF, deciduous broadleaved forest.

589 **Figure 3. Ridge regressions between seasonal vegetation growth and monthly**  
590 **autumnal runoff.** (a-c) Spatial distributions of the ridge-regression coefficients  
591 (magnitudes and directions of the effects are denoted by the values; specifically,  
592 negative coefficients indicate that vegetation greening decreases autumnal monthly  
593 runoff) between spring LAI and (a) September (Sep), (b) October (Oct) and (c)  
594 November (Nov) monthly runoff. (d) Kernel density estimates of the frequency  
595 distributions of ridge-regression coefficients across different plant functional types..  
596 (e-g) Same as (a-c) but for summer LAI. (h) Same as (d) but for summer LAI. The  
597 dashed lines represent means.

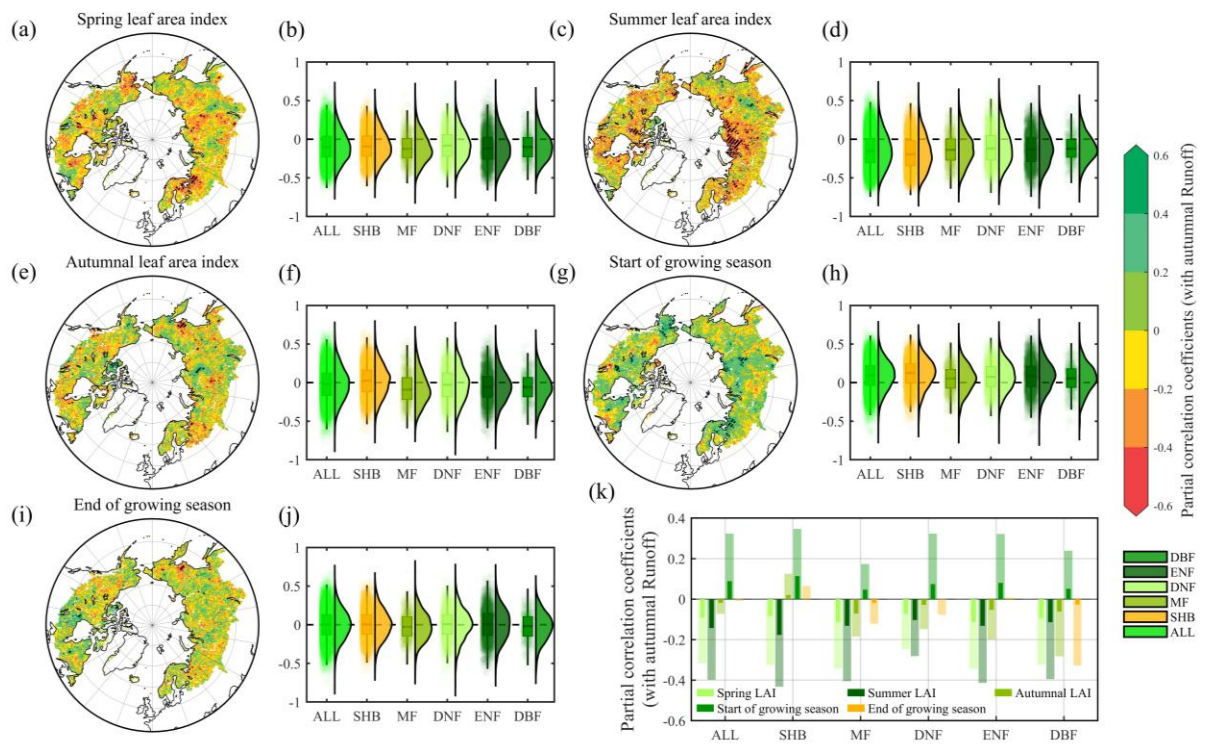
598 **Figure 4. Effects of seasonal vegetation growth on monthly runoff in autumn**  
599 **among the plant functional types.** The upper left and right heat maps show the  
600 influences of spring LAI and summer LAI on monthly runoff in autumn obtained by  
601 the ridge-regression analysis, respectively. The lower-left heat map represents the

602 effect of seasonal vegetation growth on monthly runoff in autumn isolated from the  
603 experiments using the LPJ-GUESS model forced by CRUNCEP v7 (1982-2014).

604 **Figure 5. Schematic of the impact of seasonal vegetation growth on autumnal**  
605 **runoff in regions with green summers versus regions with mixed or evergreen**  
606 **forest.** The color gradient within the gradual arrows (green-to-brown-to-gray)  
607 represents the temporal progression of phenological stages, transitioning from peak  
608 physiological activity to senescence and dormancy. This shift indicates a gradual  
609 attenuation in the vegetation's capacity to influence the water cycle over time. The  
610 blue arrows indicate the impacts of seasonal vegetation growth on elements of the  
611 water cycle, e.g. transpiration, T and runoff. Arrow length represents the magnitude of  
612 the influence. Seasonal vegetation greening in spring and summer affects autumnal  
613 runoff by affecting soil-water content (SWC) and autumnal vegetation growth by CSE.  
614 (a) In regions with green summers, the rapid decrease in LAI weakened the effects of  
615 early seasonal vegetation growth on autumnal runoff, especially in spring. (b) Early  
616 seasonal vegetation growth in regions with mixed or evergreen forest, however,  
617 continues to affect autumnal runoff.

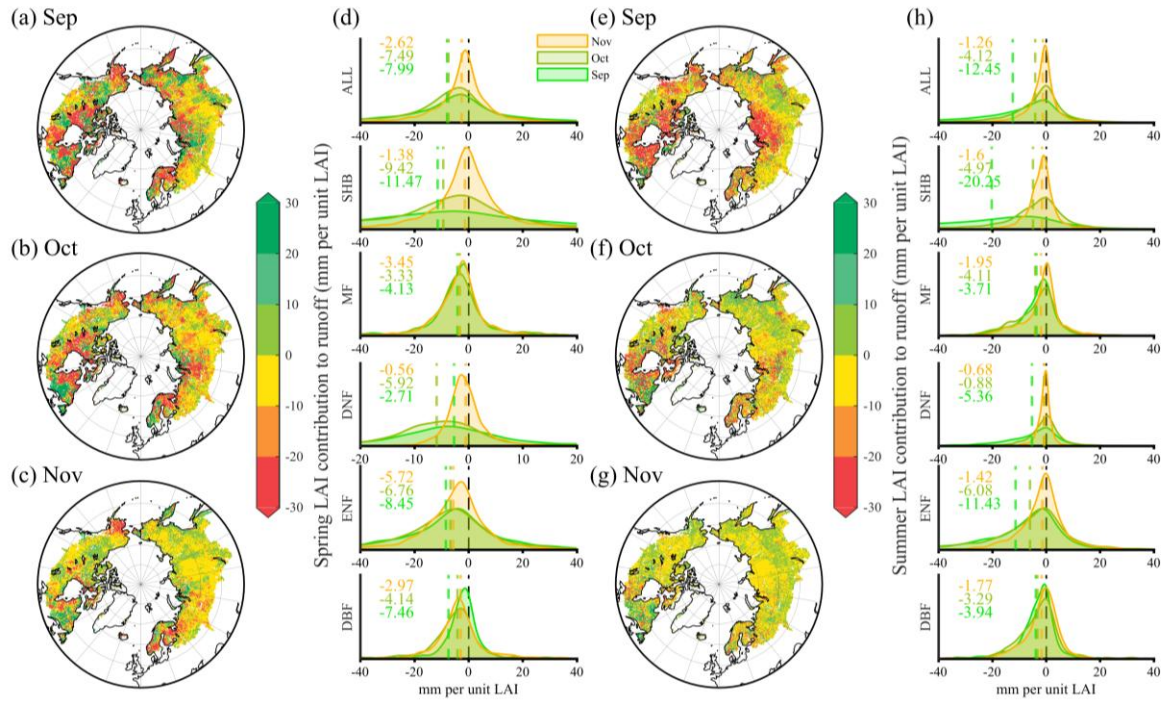


621 **Figure 2**



622

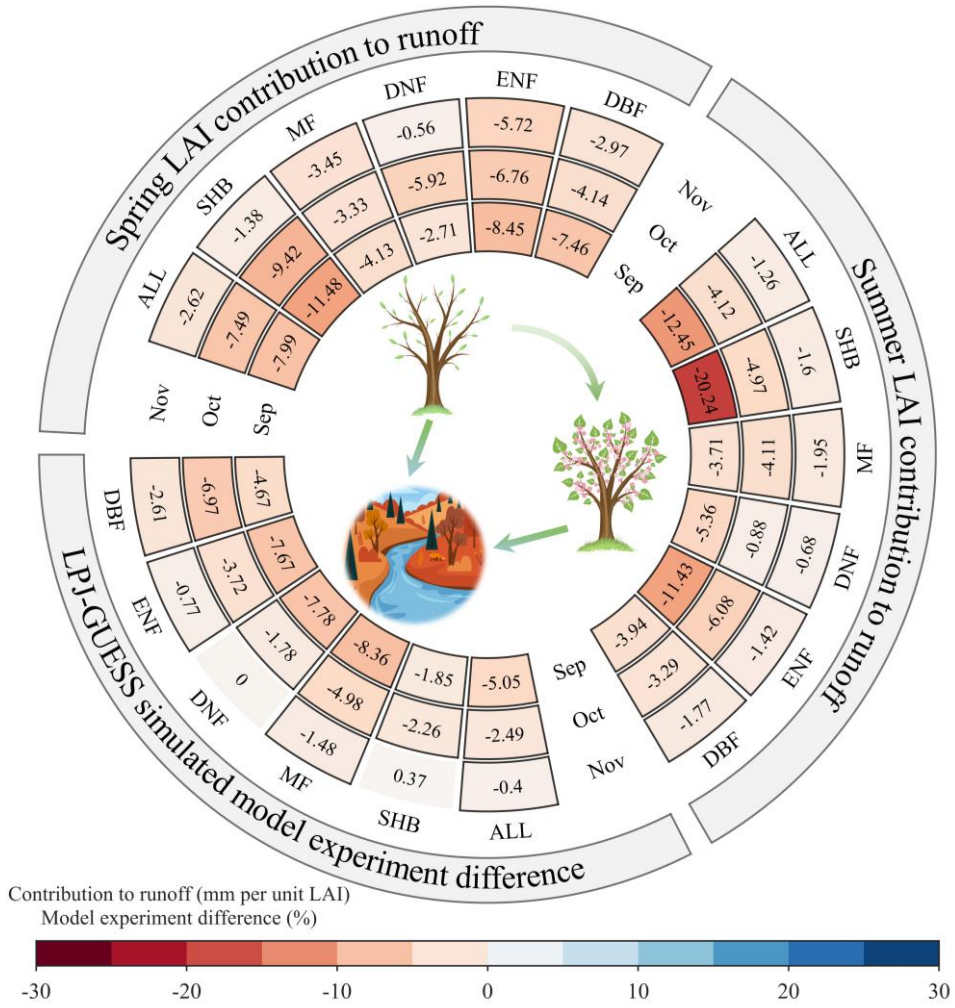
623



625

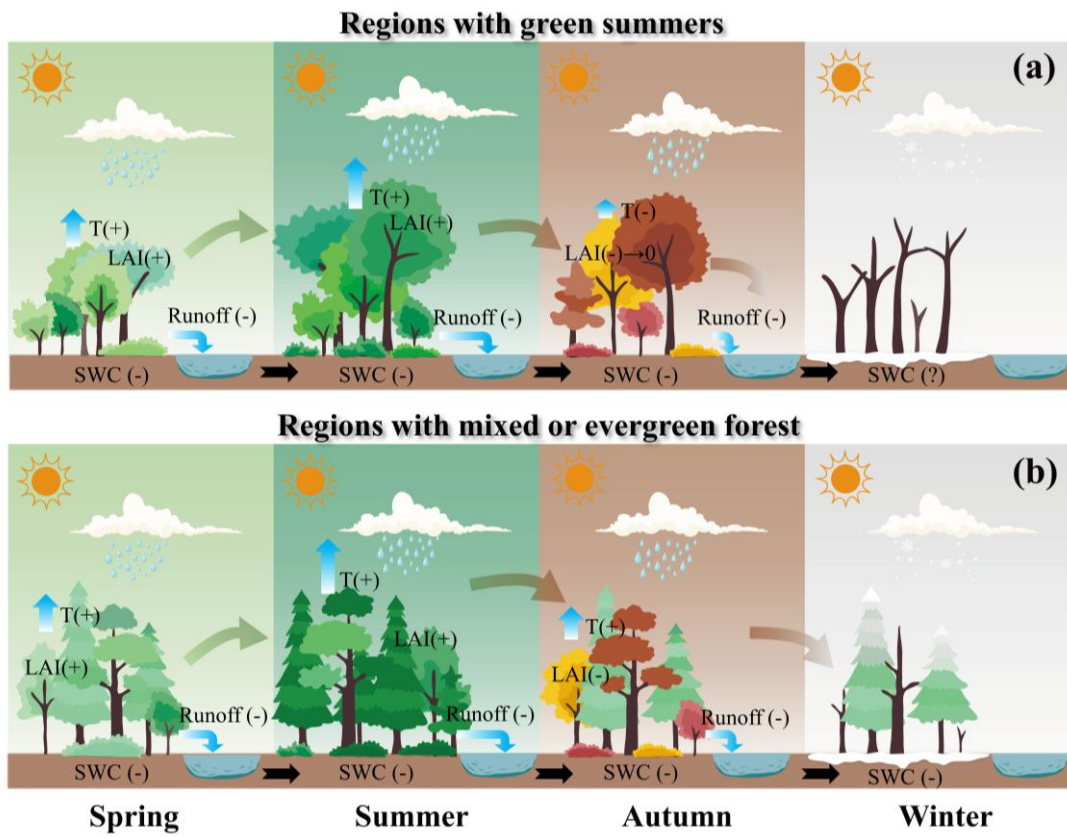
626

627 **Figure 4**



628

629



## Supplementary Files

This is a list of supplementary files associated with this preprint. Click to download.

- [Supplementarymaterial.pdf](#)